Composition of continental crust altered by the emergence of land plants

Christopher J. Spencer[1]*, Neil S. Davies[2], Thomas M. Gernon[3], Xi Wang[1], William J. McMahon[2], Taylor Rae I. Morrell[1], Thea Hincks[3], Peir K. Pufahl[1], Alexander Brasier[4], Marina Seraine[1], Gui-Mei Lu[1,5]

*Corresponding author. Email: c.spencer@queensu.ca

[1]Department of Geological Sciences and Geological Engineering, Queen's University; Kingston K7L 2N8, Ontario, Canada

[2]Department of Earth Sciences, University of Cambridge; Downing Street, Cambridge CB2 3EQ, United Kingdom

[3]School of Ocean & Earth Science, University of Southampton; Southampton SO14 3ZH, United Kingdom

[4]School of Geosciences, University of Aberdeen, King's College; Aberdeen AB24 3UE, United Kingdom

[5]State Key Laboratory of Geological Processes and Mineral Resources, School of Earth Sciences, China University of Geosciences; Wuhan 430074, China

The evolution of land plants during the Palaeozoic Era transformed Earth's biosphere. Because the Earth's surface and interior are linked by tectonic processes, the linked evolution of the biosphere and sedimentary rocks should be recorded as a near-contemporary shift in the composition of the continental crust. To test this hypothesis, we assessed the isotopic signatures of zircon formed at subduction zones where marine sediments are transported into the mantle, thereby recording interactions between surface environments and the deep Earth. Using oxygen and lutetium-hafnium isotopes of magmatic zircon that respectively track surface weathering (time-independent) and radiogenic decay (time-dependent), we find a correlation in the composition of continental crust after 430 Myr ago, which is coeval with the onset of enhanced complexity and stability in sedimentary systems related to the evolution of vascular plants. The expansion of terrestrial vegetation brought channelled sand-bed and meandering rivers, muddy floodplains, and thicker soils, lengthening the duration of weathering before final marine deposition. Collectively, our results suggest that the evolution of vascular plants coupled the degree of weathering and timescales of sediment routing to depositional basins where they were subsequently subducted and melted. The late Palaeozoic isotopic shift of zircon indicates that the greening of the continents was recorded in the deep Earth.

Plants are the dominant kingdom of life on Earth, accounting for ≈450 gigatons of a total ≈550 Gt of extant living biomass [1], and successfully colonizing ~84% surface area of the presently subaerially exposed continental crust [2]. Yet Earth's status as a 'green planet' is geologically recent, and other than some millimetre-thick microbial mats [3], terrestrial vegetation was absent for approximately 90% of the planet's history. Recently reported palynological evidence indicates that the first embryophytes (land plants) likely evolved from aquatic charophyte algae, that had begun to adapt to terrestrial settings by at least the early Ordovician (c. 480 Myr ago) [4,5]. The earliest empirical fossil evidence for vegetated continents comes from cryptospores that appear recurrently in strata onwards from the Middle Ordovician (c. 467-470 Myr ago) [6], attesting to relative evolutionary stasis in which early land plants were restricted to wet coastal environments, and maintained diminutive, low diversity, simple forms for the first 30-40 Myr of their history [7,8]. Eventually this primitive vegetation became outcompeted by vascular plants, and both spores and plant megafossils attest to a major late Silurian-Early Devonian adaptive radiation of land plants (diversification, morphological innovation and increasing size) that initiated at the end of the Llandovery Epoch (c. 433 Myr ago) [9].

Land Plants and Riverine Sediments

Early Palaeozoic land plants had profound impacts on Earth surface processes and geological products. Fossil evidence for the advent of land plants is coeval with a step increase in the amount of mudrock deposited in continental settings [10,11]. Throughout the Precambrian, terrigenous mudrocks were primarily the product of physical erosion with limited pedogenic clay mineral formation [12]. However, geochemical data suggest that in the early Palaeozoic, the primary locus of the global 'clay mineral factory' shifted from the oceans to the land [13] as early land plants induced the inception of new pathways in (micro)biologically mediated weathering. Fossil evidence supports this notion, as Silurian plants—and their bacterial and fungal symbionts—formed early plant ground covers that would have intensified clay mineral weathering [14].

The Early Devonian evolution of advanced rooting systems with root axes and meristems [15] would have caused a further increase to the volume of the critical zone for terrigenous weathering, promoting a greater root surface area and amplified connectivity with the reactive near-surface environment [16]. The increased volume of mud and clay on the continents was likely also boosted by the disruption of seaward transport of fine sediments by the retentive influences of land plants as obstacles and stabilizers [10,11,17], and possibly by the capacity of their organic matter to heighten mud flocculation and deposition [18].

Physical sedimentary processes and products on the continents were also influenced by the evolutionary adaptations of plants. Advances such as the evolution of vascular plant roots, around 411 Myr ago [15], and the earliest trees at 390-388 Myr ago [19,20], bound channel margins and increased complexity in river geomorphology at a variety of spatio-temporal scales [10]. A prominent impact is seen in the rise in abundance of mud-rich fluvial deposits during the Silurian and Devonian, distinguishing them from more ancient mud-poor alluvium and attesting to an increase in meandering river planforms [10]. Although rapidly migrating sandy meandering systems were almost certainly in existence before the evolution of land plants [10], the Silurian and Devonian ushered in the first abundant mesoscale, muddy meandering channels [21], which would have both fragmented and lengthened source-to-sink sediment conduits and maintained stable floodplains as long-lived sediment staging areas. Incorporation of the plant organic matter into floodplain sediments also affected carbon cycling, driving enhanced production of calcrete (calcium carbonate) in terrestrial sediments from the Silurian onwards [22,23]. It seems likely that the development of plants with rhizospheres in the Siluro-Devonian will also have directly enhanced chemical rock weathering [24]: a hypothesis that demands checking of suitable proxies.

The oxygen isotopic composition of the continental crust is one such proxy [25]. From the bulk Earth average $\delta^{18}O$ of ~5.5‰ (as compared to Vienna Standard Mean Ocean Water) [26], isotopic fractionation during low-temperature weathering and water-rock interaction led to elevated whole-rock $\delta^{18}O$ values in siliciclastic sedimentary rocks. Even in sparsely vegetated environments, the weathering of silicate material results in higher $\delta^{18}O$ in sediments and minimal post-depositional isotope exchange with ground or surface waters [27]. Whilst high $\delta^{18}O$ (> 15‰) were present throughout the Proterozoic Eon and exhibit a marked increase across the Archean–Proterozoic transition [28], the distribution of $\delta^{18}O$ and chemical index of alteration of non-glaciogenic mudrocks does not dramatically change throughout the Phanerozoic (Supplementary Figure 1) [28].

Conversely, empirical geologic evidence shows that the volume of continental mudrock preserved in the geologic record expanded dramatically during the early Palaeozoic [11]. Models have also predicted that the advent of land plants increased silicate weathering rates by a factor 2 to 10 (ref. [24]) albeit in a transitory way [29], and an increase in silicate weathering and increased CO_2 fixation via photosynthesis led to substantive cooling during the late Ordovician [30] and Devonian [31]. These lines of evidence suggest that associated signals could be found in under-explored archives, including Earth's zircon $\delta^{18}O$ record.

Sediment Recycling in Magmatic Systems

Sedimentary deposition along continental margins and within ocean basins ultimately leads to a global fraction of that material becoming incorporated into magmatic systems during subduction [32,33]. The most common loci of such activity are subduction zones where sedimentary material is either subducted into the asthenosphere [34], or melted in the upper crust along the periphery of rising plutons [35]. While other convergent margins also form sediment-derived magmas (e.g., continental orogens [36] and back-arc basins [37]), given the length of global subduction zones, these are likely the largest contributor of magma influenced by sedimentary material [38].

The influence of sediment on magmatic systems is most commonly tracked through geologic time using $\delta^{18}O$ and U-Pb geochronology of the mineral, zircon [39]. It is understood that any igneous rocks with $\delta^{18}O$ values divergent from the average mantle (~5.5‰) must have been in part or wholly derived from supracrustal material [39] and that the presence of a sedimentary $\delta^{18}O$ signature in magmatic zircon can be traced from some of the oldest terrestrial zircon (~4.27 Gyr ago) [40,41] to the youngest exposed granites (818.5±9.6 kyr ago) [42]. Another powerful isotopic tool in zircon is Lu-Hf, where the radioactive β-decay of ^{176}Lu to ^{176}Hf allows for comparison of the Lu-Hf isotopic composition of zircon at formation with the chondrite uniform reservoir and depleted mantle. 176Lu/177Hf is displayed as εHf that is normalized to the chondrite uniform reservoir.[43]

Tracing Sedimentary Components in Zircon

We developed a new compilation of U-Pb, Lu-Hf, and O isotopic data from detrital zircon [5] to evaluate secular change in their correlations (Fig. 1). To assess the correlation of εHf and $\delta^{18}O$ over time, we use a rolling window to visualize changes in the slope, r^2, Pearson's correlation, and Spearman's Rank correlation (Figs. 1F, 2) [5]. We find no statistically reliable correlation between εHf and $\delta^{18}O$ prior to 450 Myr ago. After ~430 Myr ago, however, εHf and $\delta^{18}O$ show a strong correlation as well as a statistically significant step change between 450-430 Myr ago (Fig. 2; Extended Data Fig. 2) [5]. Covariance in independent zircon O and Lu-Hf isotopic datasets (analyses not from the same zircon grains) has previously been linked to deglaciation and sediment subduction following the Cryogenian global glaciation [44]. In constrast, this study evaluates the correlation of O and Lu-Hf isotopes in individual zircon thus providing a unique view at the grain scale [5]. In addition, we expand upon the work of ref. [11] through the application of a step change algorithm to the percentage of mudrocks in sedimentary successions, which reveals a significant increase at 430 Myr ago (Fig. 3; Extended Data Fig. 3) in tandem with the late Silurian adaptive radiation of land plants [9]. Assessment of tectonic subdivisions using the timing of supercontinent assembly confirms that none of the periods of substantial collisional orogenesis yield a statistically significant correlation between zircon εHf and $\delta^{18}O$ (Extended Data Fig. 4) meaning that supercontinent tectonics can be ruled out as the driver of this signal [5].

The U-Pb and Lu-Hf isotope systems track magmatism and crystallization at temperatures >700ºC and thus document geologic processes occurring deep in Earth's crust and recording the chronology of magmatic processes (i.e., mantle extraction and zircon crystallization). While the oxygen isotopic compositions of zircon are also imparted within the magmatic system at depth, elevated $\delta^{18}O$ indicates the melting of material that was once exposed at Earth's surface (i.e., (meta)sedimentary material; Fig. 1A). Given that the melting of (meta)sedimentary material occurs in a multitude of magmatic rocks with sediments of varying ages [45] and different tectonic settings (e.g., young sediments in oceanic arcs; [32]; old sediments in collisional orogens; [36]), there is no prima facie expectation for Lu-Hf and O isotopes in zircon to be correlated.

The post-430 Myr ago correlation between these two magmatic proxies implies some secular change in the rates of sediment transport from source-to-sink, with the sediment sink subsequently facilitating melting of sedimentary material. Importantly, the εHf – $\delta^{18}O$ correlation requires a diversity of processes including the formation of zircon with mantle-derived isotopic signatures (both in Lu-Hf and O isotopes) along with the melting of progressively older and more highly weathered sedimentary rocks. As mantle-derived magmatism forms the endmember from which all primary crustal magmas form, the secular change discussed herein is assumed to primarily represent sedimentary processes.

Due to the time-integrated nature of εHf, the comparison of εHf and $\delta^{18}O$ through time is problematic. However, when dealing with narrow windows of time (<250 Myr) the amount of radiogenic decay in the chondrite uniform reservoir (CHUR) is minimized. An alterative assessment can be done by using crustal residence ages (depleted mantle model age minus crystallization age). This however comes with an assumption of the $^{176}Lu/^{177}Hf$ applied globally. Nevertheless, εHf versus $\delta^{18}O$ show broadly the same patterns as crustal residence versus $\delta^{18}O$ (Extended Data Fig. 5, Extended Data Fig. 6). We compare secular change of zircon compositions with sedimentological and paleontological data to quantitatively understand potential linkages between terrestrial biosphere evolution—including the expansion of vascular land plants and their influence on source-to-sink sediment transfer—to the melting of sediments in convergent margins and the composition of magmatic zircon and by proxy the continental crust.

The widespread development of post-Archean continental freeboard [46,47] and the concomitant increase in continental weathering is inferred from an increase of mudrock $\delta^{18}O$ throughout the Proterozoic [28]; no equivalent secular change is apparent in post-Proterozoic mudrocks (Extended Data Fig. 1). Therefore, the importance of progressive weathering and mudrock formation (and thus facilitation of the increase in zircon $\delta^{18}O$ when (meta)sedimentary material is melted) must also be in some way tied to the duration of time between progressive weathering (i.e., increasing $\delta^{18}O$) and sediment deposition in loci available for incorporation and melting in magmatic systems (e.g., along a subduction trench).

Connecting Land Plants and Zircon

The duration of surface weathering influences the radiogenic ingrowth of Lu-Hf isotopes and mass-dependent fractionation of oxygen isotopes, and is dependent on sediment residence time within the critical zone [48]. Sediment delivered to rivers at source is then routed through a sediment transfer system. The residence time of a pulse of sediment within this system increases with: 1) the length of the river system; 2) the number of buffers within that system where sediment undergoes transient storage and remains static (e.g., floodplains); and 3) the relative abundance of suspended bed-material load relative to bedload [49,50]. The greater sinuosity of meandering channels (compared with braided river networks) means that they are inherently longer routing systems. The associated long-lived floodplains of meandering rivers provide more robust buffers than those in laterally-mobile braided rivers [51], and sediment transport is more regularly dominated by mixed- or suspended bed-material load. Each of these considerations imply that the time taken for source-to-sink sediment transport is greater in meandering than in braided rivers. Even though individual particles of suspended sediment can be transported more rapidly than bedload within a channel [52], individual sediment particles can transit almost five times slower in meandering rivers (9.6 yr km^{-1}) than in braided rivers (1.9 yr km^{-1}) [53]. This discrepancy is largely accounted for by residence of particles within hillslope [54] and floodplain [55] staging areas, which are only re-entrained after intervals on the order of 10^4-10^5 kyr [56,57], within the timeframe of mature soil development and chemical weathering [54,55].

Relevantly, at 430 Myr ago, the empirical shift towards correlated O and Hf-Lu isotopes in zircon is coincident with a global unidirectional shift towards an increased abundance of meandering river channel morphologies (Fig. 3), as tracked by the frequency distribution to physical characteristics of alluvium archived in continental basins [10,58]. River sediments deposited after this juncture exhibit a jump in the abundance of mudrock [11] and heterolithic lateral accretion sets [21], attesting to a rise in long-lived floodplains, channel stability, and mesoscale sinuosity, that can be mechanistically explained by the novel influence of vegetation acting as a geomorphic agent [11,21]. While the specific impact of vegetation manifests at the local scale, the global aggregation of a multitude of local effects (which did not exist prior to c. 430 Myr ago) increased the probability of prolonged continental weathering, with downstream impacts on the isotopic composition of the marine sediment [13] that could be incorporated into magmatic systems [59].

Based on the considerable post-430 Myr ago increase of the zircon isotopic correlation (Lu-Hf and $\delta^{18}O$), we hypothesize a connection between the evolution of land plants and the final fate of sediment in magmatic systems. Following deposition of sedimentary successions along passive margins, these successions were then in prime placement to be subducted along accretionary margins or alternatively get caught in collisional orogens. In both scenarios, sedimentary units are metamorphosed and typically assimilated into arc magmas or melted in collisional systems. The zircon in the resulting magmas exhibit elevated $\delta^{18}O$ values due to incorporation of sediments. While elevated zircon $\delta^{18}O$ occurs as early as 4.27 Gyr ago [40,41], critically the coupling between radiogenic isotope systematics (Lu-Hf, U-Pb) and $\delta^{18}O$ in zircon is absent until after 430 Myr ago.

The unidirectional shift in both the zircon and stratigraphic record likely rules out an origin owed to cyclical or episodic geological processes (e.g., tectonic or climatic) as such phenomena have persisted across the planet from the Archean onwards [60]. The studied interval, from 1200 – 0 Myr ago includes multiple orogenies, numerous alternations between icehouse and greenhouse conditions and the assembly of two supercontinents yet, similar to the unidirectional upsurge in alluvial mudrock [11], none of these extrinsic events appear to have exerted any influence on the observed oxygen and lutetium-hafnium isotopes in zircon. The singular observable shift that does occur, and that we describe, is both coincident with—and explicable by—the onset of more complex vegetation in the late Silurian.

We propose that the evolution of land plants led to the stabilization of fluvial systems, resulting in substantial upland weathering and the formation of larger volumes of mud. The resulting higher degrees of weathering along decelerated source-to-sink sediment pathways led to higher $\delta^{18}O$ signatures in the mud deposited as mudrocks. The eventual melting of this high $\delta^{18}O$ mud led to higher $\delta^{18}O$ magmas, providing a direct link between the evolution of the nascent terrestrial biosphere and composition of the lithosphere.

Acknowledgements

This manuscript benefited greatly from discussions with Brenhin Keller. CJS, XW, MS were supported by Natural Sciences and Environment Research Council, Discovery Grant RGPIN-2020-05639. TRM was supported by Natural Sciences and Environment Research Council, Undergraduate Student Research Award 551207 – 2020. TMG and TH were supported by the Turing Institute under the EPSRC grant EP/N510129/1. NSD and WJM were supported by NERC grant NE/T00696X. GML acknowledges support from the State Scholarship Fund of China Scholarship Council (202006410023).

Author contributions:

CJS conceived of the idea and with the help of XW, TRM, MS, NSD, and WJM compiled and interpreted data. CJS, XW, TH, TMG, and GML assisted with the statistical analysis. CJS, XW, WJM, and TH constructed the figures. CJS, NSD, and TMG wrote the manuscript with input from XW, WJM, TRM, TH, PKP, AB, MS, and GML.

Competing interests:

Authors declare that they have no competing interests.

Figure Captions

Fig. 1: εHf versus $\delta^{18}O$ in zircon since 720 Myr ago (A-E). It is assumed here that all primary magmas are initially derived from the mantle with a $\delta^{18}O$ of ~5.5‰ and a crustal residence time less than ~250 Myr (approximating the depleted mantle compositions [61]). The degree of correlation between εHf and $\delta^{18}O_{zircon}$ is markedly different in the latter two panels (A & B), with the panels covering pre-430 Myr ago showing greater degrees of scatter and weak correlations. F) r^2 versus slope of the regression from 700 Myr ago to 0 Myr ago in 10 Myr steps using a rolling window [5].

Fig. 2: Statistical relationship between εHf and $\delta^{18}O$ of zircon. A step-change algorithm (conjugate partitioned recursion [5]) demonstrates a statistically valid step change in the slope, r^2 and correlation coefficients at either 450 Myr ago (linear regression slope and Pearson's Correlation) or 430 Myr ago (r^2 and Spearman's Rank Correlation). The increase in vascular plants at 450 Myr ago and the increase in mudrock percentage at 430 Myr ago are shown as vertical dashed lines.

Fig. 3: Synthesis of paleontological and sedimentological data from the early Palaeozoic. Bottom panel: percentage of mudrocks in sedimentary successions from the late Ediacaran through the Carboniferous (data from ref. [11]). We find a step change in the abundance of mudrocks at 430 Myr ago [5]. It is after this point that the correlation between zircon εHf and $\delta^{18}O$ increases considerably (Fig. 2). Middle panel: cumulative classification of fluvial rock units through the early Palaeozoic [58] showing a shift in the type and diversity of fluvial deposit

characteristics at ~430 Myr ago. Top panel: Number of vascular plant species [62] and approximate timing of the first land plants, vascular plants, deeper roots, arborescence, and seeds [63].

Fig. 4: Schematic model of fluvial systems both before and after the development of land plants. Prior to the Devonian Period, minimal land plants, rapid channel migration, and river systems dominated by braided rivers led to rapid sediment transfer, minimal development of mud-sized particles, and minor deposition of mudrocks along continental margins. In contrast, after the Devonian, the expansion of vascular land plants led to the development of meandering rivers and the dramatic slowing of sediment transfer to marine environments. These diametric depositional systems influenced the isotopic composition of sediment available for reworking and melting in magmatic systems along destructive plate boundaries.

References

1. Bar-On, Y. M., Phillips, R. & Milo, R. The biomass distribution on Earth. *Proceedings of the National Academy of Sciences* **115**, 6506–6511 (2018).
2. Corenblit, D. *et al.* Feedbacks between geomorphology and biota controlling Earth surface processes and landforms: a review of foundation concepts and current understandings. *Earth-Science Reviews* **106**, 307–331 (2011).
3. Brasier, A. T., Culwick, T., Battison, L., Callow, R. H. T. & Brasier, M. D. Evaluating evidence from the Torridonian Supergroup (Scotland, UK) for eukaryotic life on land in the Proterozoic. *Geological Society, London, Special Publications* **448**, 121–144 (2017).
4. Strother, P. K. & Foster, C. A fossil record of land plant origins from charophyte algae. *Science* **373**, 792–796 (2021).
5. Further information is available in the supplementary materials.
6. Rubinstein, C. V, Gerrienne, P., de la Puente, G. S., Astini, R. A. & Steemans, P. Early Middle Ordovician evidence for land plants in Argentina (eastern Gondwana). *New Phytologist* **188**, 365–369 (2010).
7. Wellman, C. H., Steemans, P. & Vecoli, M. Palaeophytogeography of Ordovician–Silurian land plants. *Geological Society, London, Memoirs* **38**, 461–476 (2013).
8. Harrison, C. J. & Morris, J. L. The origin and early evolution of vascular plant shoots and leaves. *Philosophical Transactions of the Royal Society B: Biological Sciences* **373**, 20160496 (2018).
9. Wellman, C. *et al.* Low tropical diversity during the adaptive radiation of early land plants. *Nature Plants* (2021).

10. Davies, N. S. & Gibling, M. R. Cambrian to Devonian evolution of alluvial systems: The sedimentological impact of the earliest land plants. *Earth-Science Reviews* **98**, 171–200 (2010).
11. McMahon, W. J. & Davies, N. S. Evolution of alluvial mudrock forced by early land plants. *Science* **359**, 1022–1024 (2018).
12. Rafiei, M. & Kennedy, M. Weathering in a world without terrestrial life recorded in the Mesoproterozoic Velkerri Formation. *Nature communications* **10**, 1–9 (2019).
13. Kalderon-Asael, B. *et al.* A lithium-isotope perspective on the evolution of carbon and silicon cycles. *Nature* **595**, 394–398 (2021).
14. Mitchell, R. L. *et al.* Cryptogamic ground covers as analogues for early terrestrial biospheres: Initiation and evolution of biologically mediated proto-soils. *Geobiology* **19**, 292–306 (2021).
15. Hetherington, A. J. & Dolan, L. Stepwise and independent origins of roots among land plants. *Nature* **561**, 235–238 (2018).
16. Moulton, K. L., West, J. & Berner, R. A. Solute flux and mineral mass balance approaches to the quantification of plant effects on silicate weathering. *American Journal of Science* **300**, 539–570 (2000).
17. Davies, N. S. & McMahon, W. J. Land plant evolution and global erosion rates. *Chemical Geology* **567**, 120128 (2021).
18. Zeichner, S. S. *et al.* Early plant organics increased global terrestrial mud deposition through enhanced flocculation. *Science* **371**, 526–529 (2021).
19. Berry, C. M. & Fairon-Demaret, M. The architecture of Pseudosporochnus nodosus Leclercq et Banks: a Middle Devonian cladoxylopsid from Belgium. *International Journal of Plant Sciences* **163**, 699–713 (2002).

20. Stein, W. E. *et al.* Mid-Devonian Archaeopteris roots signal revolutionary change in earliest fossil forests. *Current biology* **30**, 421–431 (2020).

21. Davies, N. S. & Gibling, M. R. Paleozoic vegetation and the Siluro-Devonian rise of fluvial lateral accretion sets. *Geology* **38**, 51–54 (2010).

22. Brasier, A. T. Searching for travertines, calcretes and speleothems in deep time: Processes, appearances, predictions and the impact of plants. *Earth-Science Reviews* **104**, 213–239 (2011).

23. Brasier, A. T., Morris, J. L. & Hillier, R. D. Carbon isotopic evidence for organic matter oxidation in soils of the Old Red Sandstone (Silurian to Devonian, South Wales, UK). *Journal of the Geological Society* **171**, 621–634 (2014).

24. Moulton, K. L. & Berner, R. A. Quantification of the effect of plants on weathering: Studies in Iceland. *Geology* **26**, 895–898 (1998).

25. Eiler, J. M. Oxygen isotope variations of basaltic lavas and upper mantle rocks. *Reviews in mineralogy and geochemistry* **43**, 319–364 (2001).

26. McKeegan, K. D. *et al.* The oxygen isotopic composition of the Sun inferred from captured solar wind. *Science* **332**, 1528–1532 (2011).

27. Clauer, N., O'Neil, J. R. & Bonnot-Courtois, C. The effect of natural weathering on the chemical and isotopic compositions of biotites. *Geochimica et Cosmochimica Acta* **46**, 1755–1762 (1982).

28. Bindeman, I. N., Bekker, A. & Zakharov, D. O. Oxygen isotope perspective on crustal evolution on early Earth: A record of Precambrian shales with emphasis on Paleoproterozoic glaciations and Great Oxygenation Event. *Earth and Planetary Science Letters* **437**, 101–113 (2016).

29. Lipp, A. G. *et al.* The composition and weathering of the continents over geologic time. *Geochemical Perspectives Letters* **7**, 21–26 (2021).

30. Lenton, T. M., Crouch, M., Johnson, M., Pires, N. & Dolan, L. First plants cooled the Ordovician. *Nature Geoscience* **5**, 86–89 (2012).

31. Berner, R. A. The rise of plants and their effect on weathering and atmospheric CO2. *Science* **276**, 544–546 (1997).

32. Plank, T., Kelley, K. A., Murray, R. W. & Stern, L. Q. Chemical composition of sediments subducting at the Izu-Bonin trench. *Geochemistry, Geophysics, Geosystems* **8**, (2007).

33. White, W. M. & Dupré, B. Sediment subduction and magma genesis in the Lesser Antilles: isotopic and trace element constraints. *Journal of Geophysical Research: Solid Earth* **91**, 5927–5941 (1986).

34. Spencer, C. J. *et al.* Evidence for melting mud in Earth's mantle from extreme oxygen isotope signatures in zircon. *Geology* **45**, 975–978 (2017).

35. Lackey, J. S., Valley, J. W. & Saleeby, J. B. Supracrustal input to magmas in the deep crust of Sierra Nevada batholith: Evidence from high-δ18O zircon. *Earth and Planetary Science Letters* **235**, 315–330 (2005).

36. Hopkinson, T. N. *et al.* The identification and significance of pure sediment-derived granites. *Earth and Planetary Science Letters* **467**, 57–63 (2017).

37. Kemp, A. I. S., Hawkesworth, C. J., Collins, W. J., Gray, C. M. & Blevin, P. L. Isotopic evidence for rapid continental growth in an extensional accretionary orogen: The Tasmanides, eastern Australia. *Earth and Planetary Science Letters* **284**, 455–466 (2009).

38. Bird, P. An updated digital model of plate boundaries. *Geochemistry, Geophysics, Geosystems* **4**, 1–52 (2003).

39. Valley, J. W. *et al.* 4.4 billion years of crustal maturation: Oxygen isotope ratios of magmatic zircon. *Contributions to Mineralogy and Petrology* **150**, 561–580 (2005).
40. Cavosie, A. J., Valley, J. W. & Wilde, S. A. Magmatic δ18O in 4400-3900 Ma detrital zircons: A record of the alteration and recycling of crust in the Early Archean. *Earth and Planetary Science Letters* **235**, 663–681 (2005).
41. Spencer, C. J. *et al.* Disparities in oxygen isotopes of detrital and igneous zircon identify erosional bias in crustal rock record. *Earth and Planetary Science Letters* **577**, 117248 (2022).
42. Spencer, C. J., Dani, M., Ito, H. & Hoiland, C. Rapid Exhumation of Earth ' s Youngest Exposed Granites Driven by Subduction of an Oceanic Arc Geophysical Research Letters. 1–9 (2019) doi:10.1029/2018GL080579.
43. Bouvier, A., Vervoort, J. D. & Patchett, P. J. The Lu–Hf and Sm–Nd isotopic composition of CHUR: Constraints from unequilibrated chondrites and implications for the bulk composition of terrestrial planets. *Earth and Planetary Science Letters* **273**, 48–57 (2008).
44. Keller, C. B. *et al.* Neoproterozoic glacial origin of the Great Unconformity. *Proceedings of the National Academy of Sciences of the United States of America* **116**, 1136–1145 (2019).
45. Bucholz, C. E. & Spencer, C. J. Strongly Peraluminous Granites across the Archean-Proterozoic Transition. *Journal of Petrology* **60**, 1299–1348 (2019).
46. Bindeman, I. N. *et al.* Rapid emergence of subaerial landmasses and onset of a modern hydrologic cycle 2.5 billion years ago. *Nature* **557**, 545–548 (2018).
47. Liebmann, J. *et al.* Emergence of continents above sea-level influences sediment melt composition. *Terra Nova* (2021) doi:10.1111/ter.12531.
48. Giardino, J. R. & Houser, C. Introduction to the critical zone. in *Developments in earth surface processes* vol. 19 1–13 (Elsevier, 2015).

49. Castelltort, S. & Van Den Driessche, J. How plausible are high-frequency sediment supply-driven cycles in the stratigraphic record? *Sedimentary geology* **157**, 3–13 (2003).
50. Tofelde, S., Bernhardt, A., Guerit, L. & Romans, B. W. Times associated with source-to-sink propagation of environmental signals during landscape transience. *Frontiers in Earth Science* **9**, 227 (2021).
51. Bufe, A. *et al.* Controls on the lateral channel-migration rate of braided channel systems in coarse non-cohesive sediment. *Earth Surface processes and landforms* **44**, 2823–2836 (2019).
52. Clift, P. D. & Giosan, L. Sediment fluxes and buffering in the post-glacial Indus Basin. *Basin Research* **26**, 369–386 (2014).
53. Repasch, M. *et al.* Sediment transit time and floodplain storage dynamics in alluvial rivers revealed by meteoric 10Be. *Journal of Geophysical Research: Earth Surface* **125**, e2019JF005419 (2020).
54. Suresh, P. O., Dosseto, A., Hesse, P. P. & Handley, H. K. Very long hillslope transport timescales determined from uranium-series isotopes in river sediments from a large, tectonically stable catchment. *Geochimica et Cosmochimica Acta* **142**, 442–457 (2014).
55. Li, C. *et al.* The time scale of river sediment source-to-sink processes in East Asia. *Chemical Geology* **446**, 138–146 (2016).
56. Sheldon, N. D. & Tabor, N. J. Quantitative paleoenvironmental and paleoclimatic reconstruction using paleosols. *Earth-science reviews* **95**, 1–52 (2009).
57. Ben-Israel, M., Armon, M., Team, A. & Matmon, A. Sediment Residence Times in Large Rivers Quantified Using a Cosmogenic Nuclides Based Transport Model and Implications for Buffering of Continental Erosion Signals. *Journal of Geophysical Research: Earth Surface* e2021JF006417.

58. Gibling, M. R. & Davies, N. S. Palaeozoic landscapes shaped by plant evolution. *Nature Geoscience* **5**, 99–105 (2012).

59. Plank, T. & Langmuir, C. H. Tracing trace elements from sediment input to volcanic output at subduction zones. *Nature* **362**, 739–743 (1993).

60. Davies, N. S. *et al.* Discussion on 'Tectonic and environmental controls on Palaeozoic fluvial environments: Reassessing the impacts of early land plants on sedimentation' Journal of the Geological Society, London, https://doi.org/10.1144/jgs2016-063. *Journal of the Geological Society* **174**, 947–950 (2017).

61. Jacobsen, S. B. Isotopic constraints on crustal growth and recycling. *Earth and Planetary Science Letters* **90**, 315–329 (1988).

62. Niklas, K. J., Tiffney, B. H. & Knoll, A. H. Patterns in vascular land plant diversification. *Nature* **303**, 614–616 (1983).

63. Dahl, T. W. & Arens, S. K. M. The impacts of land plant evolution on Earth's climate and oxygenation state – An interdisciplinary review. *Chemical Geology* **547**, 119665 (2020).

64. Spencer, C. J., Kirkland, C. L. & Taylor, R. J. M. Strategies towards statistically robust interpretations of in situ U-Pb zircon geochronology. *Geoscience Frontiers* **7**, 581–589 (2016).

65. Spencer, C. J., Kirkland, C. L., Roberts, N. M. W., Evans, N. J. & Liebmann, J. Strategies towards robust interpretations of in situ zircon Lu–Hf isotope analyses. *Geoscience Frontiers* **11**, 843–853 (2020).

66. Liebmann, J., Spencer, C. J., Kirkland, C. L., Xia, X. P. & Bourdet, J. Effect of water on δ18O in zircon. *Chemical Geology* **574**, 120243 (2021).

67. Spencer, C. J. *et al.* Paleoproterozoic increase in zircon δ18O driven by rapid emergence of continental crust. *Geochimica et Cosmochimica Acta* **257**, 16–25 (2019).

68. Jensen, G. *Closed-form estimation of multiple change-point models*. *PeerJ Preprints* (2013) doi:10.7287/peerj.preprints.90v3.

69. Gallagher, K. *et al.* Inference of abrupt changes in noisy geochemical records using transdimensional changepoint models. *Earth and Planetary Science Letters* **311**, 182–194 (2011).

70. Vervoort, J. D. & Kemp, A. I. S. Clarifying the zircon Hf isotope record of crust-mantle evolution. *Chemical Geology* **425**, 65–75 (2016).

71. Roberts, N. M. W. & Spencer, C. J. The zircon archive of continent formation through time. in *Geological Society Special Publication* (eds. Roberts, N. M. W., Van Kranendonk, M. J., Parman, S. W., Shirey, S. B. & Clift, P. D.) vol. 389 197–225 (2015).

72. Budd, G. E. & Mann, R. P. History is written by the victors: the effect of the push of the past on the fossil record. *Evolution* **72**, 2276–2291 (2018).

73. Cunningham, J. A., Liu, A. G., Bengtson, S. & Donoghue, P. C. J. The origin of animals: can molecular clocks and the fossil record be reconciled? *BioEssays* **39**, 1–12 (2017).

74. Dos Reis, M. *et al.* Uncertainty in the timing of origin of animals and the limits of precision in molecular timescales. *Current biology* **25**, 2939–2950 (2015).

75. Husson, J. M. & Peters, S. E. Nature of the sedimentary rock record and its implications for Earth system evolution. *Emerging Topics in Life Sciences* **2**, 125–136 (2018).

76. Donoghue, P. C. J., Harrison, C. J., Paps, J. & Schneider, H. The evolutionary emergence of land plants. *Current Biology* **31**, R1281–R1298 (2021).

77. Roberts, N. M. W. & Spencer, C. J. The zircon archive of continent formation through time. *Geological Society, London, Special Publications* **389**, 197–225 (2015).

78. Spencer, C. *et al.* Disparities in oxygen isotopes of detrital and igneous zircon identify erosional bias in crustal rock record. *Earth and Planetary Science Letters* **577**, 117248 (2022).

Correspondence and requests for materials should be addressed to CJS.

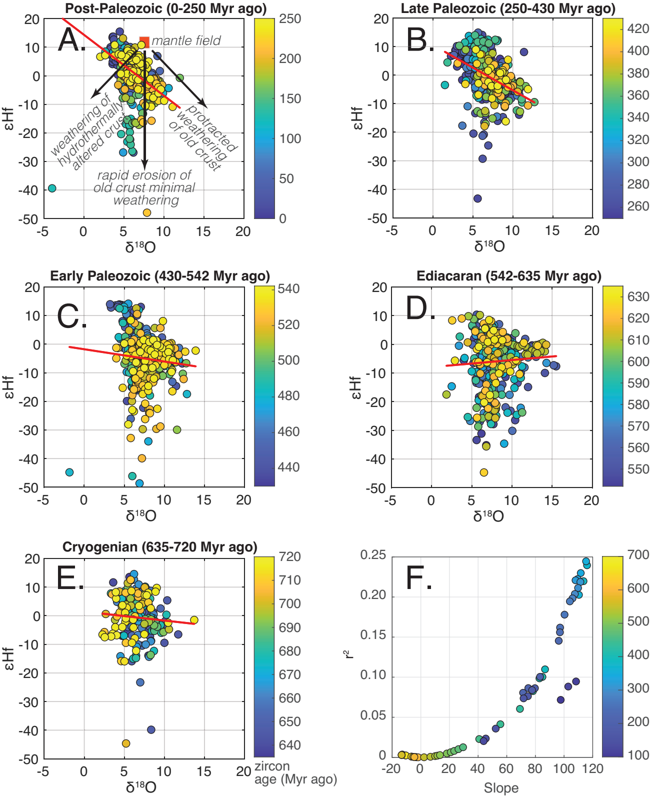

Post-Paleozoic (0-250 Myr ago)
A.
mantle field
weathering of hydrothermally altered crust
protracted weathering of old crust
rapid erosion of old crust minimal weathering
εHf
δ18O
Late Paleozoic (250-430 Myr ago)
B.
Early Paleozoic (430-542 Myr ago)
C.
Ediacaran (542-635 Myr ago)
D.
Cryogenian (635-720 Myr ago)
E.
zircon age (Myr ago)
F.
r2
Slope

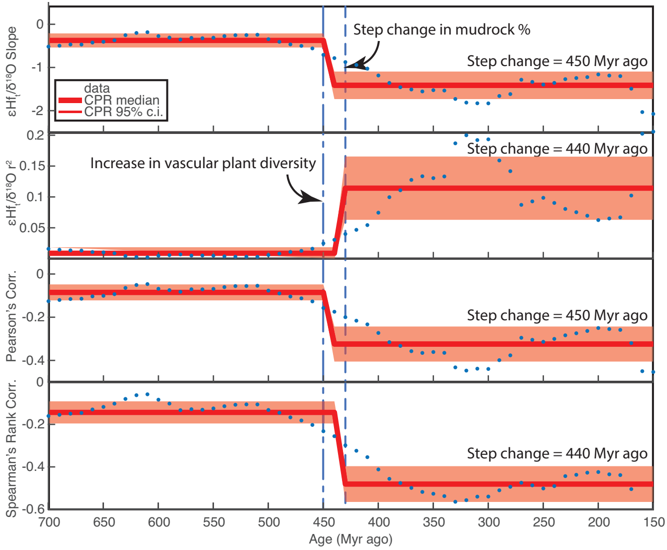

εHf$_t$/δ^{18}O Slope
Step change in mudrock %
Step change = 450 Myr ago
data
CPR median
CPR 95% c.i.
εHf$_t$/δ^{18}O r^2
Step change = 440 Myr ago
Increase in vascular plant diversity
Pearson's Corr.
Step change = 450 Myr ago
Spearman's Rank Corr.
Step change = 440 Myr ago
Age (Myr ago)

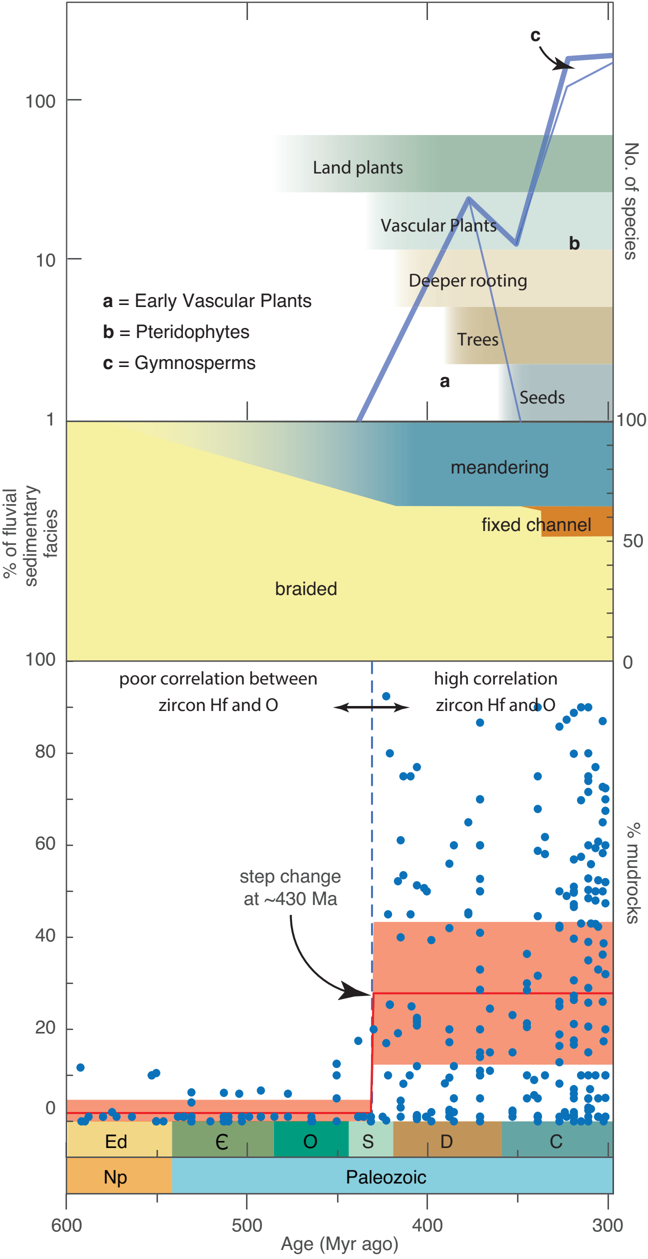

c
100
10
1
Land plants
Vascular Plants
Deeper rooting
Trees
Seeds
b
a
a = Early Vascular Plants
b = Pteridophytes
c = Gymnosperms
No. of species
100
50
0
meandering
fixed channel
braided
% of fluvial sedimentary facies
100
poor correlation between zircon Hf and O
high correlation zircon Hf and O
80
60
40
20
0
step change at ~430 Ma
% mudrocks
Ed
Є
O
S
D
C
Np
Paleozoic
600
500
400
300
Age (Myr ago)

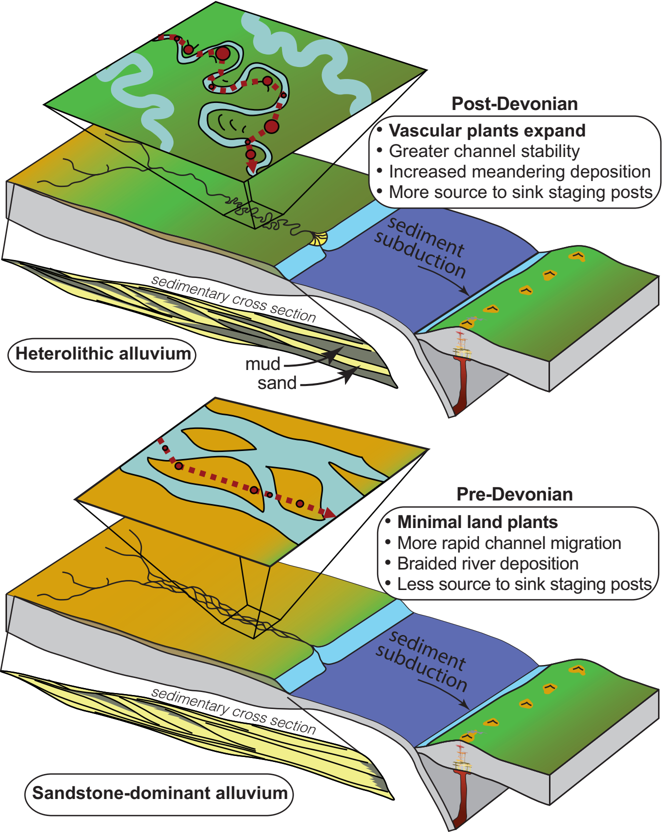
Post-Devonian
• Vascular plants expand
• Greater channel stability
• Increased meandering deposition
• More source to sink staging posts
sediment subduction
sedimentary cross section
Heterolithic alluvium
mud
sand
Pre-Devonian
• Minimal land plants
• More rapid channel migration
• Braided river deposition
• Less source to sink staging posts
sediment subduction
sedimentary cross section
Sandstone-dominant alluvium

Methods

Data Compilation

Data were compiled from 183 publications (Data S1) that included U-Pb, Lu-Hf, and O isotopic analyses of detrital zircon. Only data that passed strict quality control (concordant U-Pb ages [64], accurate stable Hf isotope ratios [65], and reliable $\delta^{18}O$ analyses [66]) were included in our analysis. U-Pb ages, $\varepsilon Hf_{(t)}$, and 2-stage depleted mantle model ages were recalculated using published isotopic ratios using unified decay constants and initial chondritic and depleted mantle values [67]. Crustal residence times (CR) were calculated by subtracting the U-Pb age from the depleted mantle model age.

Statistical Methods

We used a rolling window to visualize the change over time in the linear regression slope and R^2 values for CR and $\delta^{18}O$, and similarly the change in correlation coefficient (Pearson and Spearman's Rank) between CR and $\delta^{18}O$, and in a separate test, between zircon εHf and $\delta^{18}O$ through time (Extended Data Fig. 6).

For our purposes, the input time series do not need to be regular; the only requirement is that values for both parameters (CR and $\delta^{18}O$) exist at any given time step in the time series. We define a window width "w" (e.g., 100 Myr), an increment "i" (e.g., 5 Myr; this is the interval at which we repeat the calculations), and a start and end time.

This gives an output timeseries *t*, from start to end at increments *i*. At every time step *t*, we select the data for CR and $\delta^{18}O$ that lie within the time interval [t-(w/2), t+(w/2)]; i.e., a symmetric window centred on *t*. We then simply calculate the linear regression slope and R^2 value for CR and $\delta^{18}O$ (and separately for zircon εHf and $\delta^{18}O$) using the R function "*lm*":

$$linear\_model = lm(CR \sim \delta^{18}O)$$

The correlation is calculated using the R function, “cor”:

Pearson_correlation=cor(δ^{18}O,CR)

Spearman_correlation=cor(δ^{18}O,CR, method=”spearman”)

This process is repeated for all time steps. Note the windows overlap and are centred on the time given on the x axis in the plots shown in figure 2.

We next used conjugate partitioned recursion (CPR) to evaluate the potential presence of step changes in the linear regression slope, r^2 and correlation coefficients (Fig. 2). This iterative algorithm uses binary partitioning by marginal likelihood and conjugate priors (conjugate partition recursion) to identify an unknown number of change-points [68]. If the marginal likelihood favours a change-point model, then the algorithm defines a change point and two-sigma uncertainty bounds of the two averages before and after the change point. In applying the CPR algorithm to the correlation statistics data, we identify change-points at 450 Myr ago for εHf and δ^{18}O slope and Pearson’s correlation, and 430 Myr ago for εHf and δ^{18}O r^2 and Spearman’s rank correlation. We also performed CPR to demonstrate the presence of a change-point in the percentage of mudrocks in fluvial sequences using the data of ref. [11] (Fig. 3).

To further demonstrate the robustness of the change points described above, we also applied a Bayesian change point algorithm using transdimensional Markov chain Monte Carlo [69]. This method infers probability distributions based on the number and locations of changepoints, and the mean values between changepoints. It uses not just a single set of model parameters, but is computed using 10E6 simulations from the probability distribution to evaluate the position of the change points through time using the slope of the regression, r^2 of the regression, Pearson’s correlation, and Spearman’s rank correlation together in its identification of potential change points (Extended Data Fig. 3).

<u>*εHf versus crustal residence ages*</u>

As εHf is time integrative, comparing εHf values at different ages result is strictly invalid (e.g. εHf = 0 at 200 Ma is not equivalent to εHf = 0 at 100 Ma). However, given the narrow windows of time used in this study (<250 Myr), the difference is negligible within our interpretive framework. To address this, we also applied our statistical methods to crustal residence ages compared to $\delta^{18}O$ through time. Crustal residence time is calculated here as the difference between the U-Pb age and the projected "model age" where the radioactive decay trajectory (controlled by $^{176}Lu/^{177}Hf$) intersects with the depleted mantle [70]. This provides an estimate of how much time elapsed between the initial extraction (or melting) of the mantle and crystallization of zircon. It is important to note that crustal residence times are not geologic ages and are directly tied to depleted mantle model ages. The crustal residence time is generally low when magmas are extracted directly from mantle with zircon forming relatively rapidly, as in subduction zones. In contrast, the crustal residence time is high when ancient crust is remelted 100's of Myrs to ~4 Gyr after initial extraction from the mantle [71].

Timing of plant evolution

Here we pinpoint the timing of land plant colonization primarily based on the fossil record. While alternative suggestions of the onset of greening, arising from molecular phylogenies of living plants, suggest an earlier start to the process, there are reasons to be cautious for the statistical biases inherent in these modelling approaches [72]. A counterargument has been made that molecular phylogenies are closer to the truth for estimating timing because the paucity of non-marine strata in the Cambrian and Ordovician renders its fossil record unreliable; either because that record has been subducted [73] or because there was a limited continental area during the interval [74]. Both of these arguments are problematic: firstly, because empirically there is no exponential decay of non-marine strata with age, as sometimes envisaged by molecular phylogenists [75], and secondly because the abundance of small continents with wide continental shelves during that interval is well suited for preserved fossil evidence for land plants, as the best early record of such comes from dispersed spores preserved in shallow marine strata [6]. The fossil record thus likely provides a robust estimate of the onset of greening and, regardless, molecular clock analyses and fossil evidence are increasingly convergent on the timing of embryophyte (land plant) origins. Molecular clocks suggest that embryophytes emerged in a mid-Cambrian to Early Ordovician interval [76]. Recent palynologic evidence favours the end of this bracket and indicates that ancestral embryophytes began evolving from freshwater aquatic charophyte algae around the Early Ordovician (c. 480 Myr ago) [4].

Covariance and correlation of Lu-Hf and O isotopes

Keller et al. (2019) reported the covariance between Lu-Hf and O isotopes in zircon. This study used two separate databases that respectively reported Lu-Hf and O isotopes in zircon. They identified a large covariance peak that coincided with the timing of Cryogenian global glaciation and argued in favour of a connection between glaciogenic erosion and the composition of zircon that came from magmas influenced by the assimilation of the resulting flux of glaciogenic sediment into magmatic systems. Their numerical analysis also displayed a second peak of covariance that coincides with the evolution and proliferation of land plants that is the topic of the present study. Although this second Palaeozoic peak in zircon Lu-Hf and O covariance is more prominent in the Keller et al. (2019) study, it was not discussed. Importantly, covariance, as used in the Keller et al. (2019) study, refers to the extent to which two random variables change in tandem. For example, when the slope of secular change in Lu-Hf isotopes and $\delta^{18}O$ are changing at the same rate then covariance is high. In contrast, correlation measures strength and direction of the linear relationship between two variables. Importantly, it is not possible to measure the strength (or quality) of the linear relationship when using covariance. The Keller et al. study evaluates how Lu-Hf isotopes and $\delta^{18}O$ change in tandem using independent datasets whereas our study aims to evaluate how strongly Lu-Hf isotopes and $\delta^{18}O$ are directly correlated through time. Interestingly, our study also shows a minor increase in the strength of correlation within the timeframe of the Snowball Earth – however an increase that is a factor of five smaller than the increase in correlation associated with the rise of land plants.

Keller et al. (2019) use independent εHf and $\delta^{18}O$ datasets, that is, they use two separate databases for the two isotopic systems. This means their interpretation is limited to a comparison between the secular changes in each dataset and they are unable to directly compare Lu-Hf isotopes and $\delta^{18}O$ for specific zircon grains. In contrast, our dataset uses only Lu-Hf isotopes and $\delta^{18}O$ from the same zircon grain providing improved discriminating power in discerning secular changes in the data, which we argue is essential for our purposes. It is assumed each dataset is independently representative, which has previously been demonstrated as not being the case for Lu-Hf isotopes [77]. Further, a later compilation of zircon $\delta^{18}O$ has shown a significant bias between detrital and igneous zircon [78] which are indiscriminately combined in Keller et al. (2019). We seek to overcome these issues by comparing Lu-Hf and O isotopes from specific zircon grains.

The Keller et al. (2019) study reports two significant peaks in $\delta^{18}O$ and εHf covariance, one at ~650 Ma and the other with higher covariance at ~420 Ma. While they show both peaks in their figure 2, they omit the ~420 Ma peak from their discussion. They posit the ~650 Ma covariance*slope peak is associated with "increasing crustal reworking", while the large negative covariance*slope trough at ~420 Ma is associated with "decreasing crustal reworking". N.B. that while they state in the figure caption that a large negative covariance*slope is associated with decreased crustal reworking, they do not state the age of this trough, nor speculate on a potential cause. We posit this ~420 Ma covariance peak is supportive of our hypothesis that the evolution of land plants influenced the covariance of Lu-Hf and O isotopes in zircon.

Methods References:

1. Bar-On, Y. M., Phillips, R. & Milo, R. The biomass distribution on Earth. *Proceedings of the National Academy of Sciences* **115**, 6506–6511 (2018).
2. Corenblit, D. *et al.* Feedbacks between geomorphology and biota controlling Earth surface processes and landforms: a review of foundation concepts and current understandings. *Earth-Science Reviews* **106**, 307–331 (2011).
3. Brasier, A. T., Culwick, T., Battison, L., Callow, R. H. T. & Brasier, M. D. Evaluating evidence from the Torridonian Supergroup (Scotland, UK) for eukaryotic life on land in the Proterozoic. *Geological Society, London, Special Publications* **448**, 121–144 (2017).
4. Strother, P. K. & Foster, C. A fossil record of land plant origins from charophyte algae. *Science* **373**, 792–796 (2021).
5. Further information is available in the supplementary materials.
6. Rubinstein, C. V, Gerrienne, P., de la Puente, G. S., Astini, R. A. & Steemans, P. Early Middle Ordovician evidence for land plants in Argentina (eastern Gondwana). *New Phytologist* **188**, 365–369 (2010).
7. Wellman, C. H., Steemans, P. & Vecoli, M. Palaeophytogeography of Ordovician–Silurian land plants. *Geological Society, London, Memoirs* **38**, 461–476 (2013).
8. Harrison, C. J. & Morris, J. L. The origin and early evolution of vascular plant shoots and leaves. *Philosophical Transactions of the Royal Society B: Biological Sciences* **373**, 20160496 (2018).
9. Wellman, C. *et al.* Low tropical diversity during the adaptive radiation of early land plants. *Nature Plants* (2021).

10. Davies, N. S. & Gibling, M. R. Cambrian to Devonian evolution of alluvial systems: The sedimentological impact of the earliest land plants. *Earth-Science Reviews* **98**, 171–200 (2010).
11. McMahon, W. J. & Davies, N. S. Evolution of alluvial mudrock forced by early land plants. *Science* **359**, 1022–1024 (2018).
12. Rafiei, M. & Kennedy, M. Weathering in a world without terrestrial life recorded in the Mesoproterozoic Velkerri Formation. *Nature communications* **10**, 1–9 (2019).
13. Kalderon-Asael, B. *et al.* A lithium-isotope perspective on the evolution of carbon and silicon cycles. *Nature* **595**, 394–398 (2021).
14. Mitchell, R. L. *et al.* Cryptogamic ground covers as analogues for early terrestrial biospheres: Initiation and evolution of biologically mediated proto-soils. *Geobiology* **19**, 292–306 (2021).
15. Hetherington, A. J. & Dolan, L. Stepwise and independent origins of roots among land plants. *Nature* **561**, 235–238 (2018).
16. Moulton, K. L., West, J. & Berner, R. A. Solute flux and mineral mass balance approaches to the quantification of plant effects on silicate weathering. *American Journal of Science* **300**, 539–570 (2000).
17. Davies, N. S. & McMahon, W. J. Land plant evolution and global erosion rates. *Chemical Geology* **567**, 120128 (2021).
18. Zeichner, S. S. *et al.* Early plant organics increased global terrestrial mud deposition through enhanced flocculation. *Science* **371**, 526–529 (2021).
19. Berry, C. M. & Fairon-Demaret, M. The architecture of Pseudosporochnus nodosus Leclercq et Banks: a Middle Devonian cladoxylopsid from Belgium. *International Journal of Plant Sciences* **163**, 699–713 (2002).

20. Stein, W. E. *et al.* Mid-Devonian Archaeopteris roots signal revolutionary change in earliest fossil forests. *Current biology* **30**, 421–431 (2020).

21. Davies, N. S. & Gibling, M. R. Paleozoic vegetation and the Siluro-Devonian rise of fluvial lateral accretion sets. *Geology* **38**, 51–54 (2010).

22. Brasier, A. T. Searching for travertines, calcretes and speleothems in deep time: Processes, appearances, predictions and the impact of plants. *Earth-Science Reviews* **104**, 213–239 (2011).

23. Brasier, A. T., Morris, J. L. & Hillier, R. D. Carbon isotopic evidence for organic matter oxidation in soils of the Old Red Sandstone (Silurian to Devonian, South Wales, UK). *Journal of the Geological Society* **171**, 621–634 (2014).

24. Moulton, K. L. & Berner, R. A. Quantification of the effect of plants on weathering: Studies in Iceland. *Geology* **26**, 895–898 (1998).

25. Eiler, J. M. Oxygen isotope variations of basaltic lavas and upper mantle rocks. *Reviews in mineralogy and geochemistry* **43**, 319–364 (2001).

26. McKeegan, K. D. *et al.* The oxygen isotopic composition of the Sun inferred from captured solar wind. *Science* **332**, 1528–1532 (2011).

27. Clauer, N., O'Neil, J. R. & Bonnot-Courtois, C. The effect of natural weathering on the chemical and isotopic compositions of biotites. *Geochimica et Cosmochimica Acta* **46**, 1755–1762 (1982).

28. Bindeman, I. N., Bekker, A. & Zakharov, D. O. Oxygen isotope perspective on crustal evolution on early Earth: A record of Precambrian shales with emphasis on Paleoproterozoic glaciations and Great Oxygenation Event. *Earth and Planetary Science Letters* **437**, 101–113 (2016).

29. Lipp, A. G. *et al.* The composition and weathering of the continents over geologic time. *Geochemical Perspectives Letters* **7**, 21–26 (2021).

30. Lenton, T. M., Crouch, M., Johnson, M., Pires, N. & Dolan, L. First plants cooled the Ordovician. *Nature Geoscience* **5**, 86–89 (2012).

31. Berner, R. A. The rise of plants and their effect on weathering and atmospheric CO2. *Science* **276**, 544–546 (1997).

32. Plank, T., Kelley, K. A., Murray, R. W. & Stern, L. Q. Chemical composition of sediments subducting at the Izu-Bonin trench. *Geochemistry, Geophysics, Geosystems* **8**, (2007).

33. White, W. M. & Dupré, B. Sediment subduction and magma genesis in the Lesser Antilles: isotopic and trace element constraints. *Journal of Geophysical Research: Solid Earth* **91**, 5927–5941 (1986).

34. Spencer, C. J. *et al.* Evidence for melting mud in Earth's mantle from extreme oxygen isotope signatures in zircon. *Geology* **45**, 975–978 (2017).

35. Lackey, J. S., Valley, J. W. & Saleeby, J. B. Supracrustal input to magmas in the deep crust of Sierra Nevada batholith: Evidence from high-δ18O zircon. *Earth and Planetary Science Letters* **235**, 315–330 (2005).

36. Hopkinson, T. N. *et al.* The identification and significance of pure sediment-derived granites. *Earth and Planetary Science Letters* **467**, 57–63 (2017).

37. Kemp, A. I. S., Hawkesworth, C. J., Collins, W. J., Gray, C. M. & Blevin, P. L. Isotopic evidence for rapid continental growth in an extensional accretionary orogen: The Tasmanides, eastern Australia. *Earth and Planetary Science Letters* **284**, 455–466 (2009).

38. Bird, P. An updated digital model of plate boundaries. *Geochemistry, Geophysics, Geosystems* **4**, 1–52 (2003).

39. Valley, J. W. *et al.* 4.4 billion years of crustal maturation: Oxygen isotope ratios of magmatic zircon. *Contributions to Mineralogy and Petrology* **150**, 561–580 (2005).
40. Cavosie, A. J., Valley, J. W. & Wilde, S. A. Magmatic δ18O in 4400-3900 Ma detrital zircons: A record of the alteration and recycling of crust in the Early Archean. *Earth and Planetary Science Letters* **235**, 663–681 (2005).
41. Spencer, C. J. *et al.* Disparities in oxygen isotopes of detrital and igneous zircon identify erosional bias in crustal rock record. *Earth and Planetary Science Letters* **577**, 117248 (2022).
42. Spencer, C. J., Dani, M., Ito, H. & Hoiland, C. Rapid Exhumation of Earth ' s Youngest Exposed Granites Driven by Subduction of an Oceanic Arc Geophysical Research Letters. 1–9 (2019) doi:10.1029/2018GL080579.
43. Bouvier, A., Vervoort, J. D. & Patchett, P. J. The Lu–Hf and Sm–Nd isotopic composition of CHUR: Constraints from unequilibrated chondrites and implications for the bulk composition of terrestrial planets. *Earth and Planetary Science Letters* **273**, 48–57 (2008).
44. Keller, C. B. *et al.* Neoproterozoic glacial origin of the Great Unconformity. *Proceedings of the National Academy of Sciences of the United States of America* **116**, 1136–1145 (2019).
45. Bucholz, C. E. & Spencer, C. J. Strongly Peraluminous Granites across the Archean-Proterozoic Transition. *Journal of Petrology* **60**, 1299–1348 (2019).
46. Bindeman, I. N. *et al.* Rapid emergence of subaerial landmasses and onset of a modern hydrologic cycle 2.5 billion years ago. *Nature* **557**, 545–548 (2018).
47. Liebmann, J. *et al.* Emergence of continents above sea-level influences sediment melt composition. *Terra Nova* (2021) doi:10.1111/ter.12531.
48. Giardino, J. R. & Houser, C. Introduction to the critical zone. in *Developments in earth surface processes* vol. 19 1–13 (Elsevier, 2015).

49. Castelltort, S. & Van Den Driessche, J. How plausible are high-frequency sediment supply-driven cycles in the stratigraphic record? *Sedimentary geology* **157**, 3–13 (2003).

50. Tofelde, S., Bernhardt, A., Guerit, L. & Romans, B. W. Times associated with source-to-sink propagation of environmental signals during landscape transience. *Frontiers in Earth Science* **9**, 227 (2021).

51. Bufe, A. *et al.* Controls on the lateral channel-migration rate of braided channel systems in coarse non-cohesive sediment. *Earth Surface processes and landforms* **44**, 2823–2836 (2019).

52. Clift, P. D. & Giosan, L. Sediment fluxes and buffering in the post-glacial Indus Basin. *Basin Research* **26**, 369–386 (2014).

53. Repasch, M. *et al.* Sediment transit time and floodplain storage dynamics in alluvial rivers revealed by meteoric 10Be. *Journal of Geophysical Research: Earth Surface* **125**, e2019JF005419 (2020).

54. Suresh, P. O., Dosseto, A., Hesse, P. P. & Handley, H. K. Very long hillslope transport timescales determined from uranium-series isotopes in river sediments from a large, tectonically stable catchment. *Geochimica et Cosmochimica Acta* **142**, 442–457 (2014).

55. Li, C. *et al.* The time scale of river sediment source-to-sink processes in East Asia. *Chemical Geology* **446**, 138–146 (2016).

56. Sheldon, N. D. & Tabor, N. J. Quantitative paleoenvironmental and paleoclimatic reconstruction using paleosols. *Earth-science reviews* **95**, 1–52 (2009).

57. Ben-Israel, M., Armon, M., Team, A. & Matmon, A. Sediment Residence Times in Large Rivers Quantified Using a Cosmogenic Nuclides Based Transport Model and Implications for Buffering of Continental Erosion Signals. *Journal of Geophysical Research: Earth Surface* e2021JF006417.

58. Gibling, M. R. & Davies, N. S. Palaeozoic landscapes shaped by plant evolution. *Nature Geoscience* **5**, 99–105 (2012).

59. Plank, T. & Langmuir, C. H. Tracing trace elements from sediment input to volcanic output at subduction zones. *Nature* **362**, 739–743 (1993).

60. Davies, N. S. *et al.* Discussion on 'Tectonic and environmental controls on Palaeozoic fluvial environments: Reassessing the impacts of early land plants on sedimentation' Journal of the Geological Society, London, https://doi.org/10.1144/jgs2016-063. *Journal of the Geological Society* **174**, 947–950 (2017).

61. Jacobsen, S. B. Isotopic constraints on crustal growth and recycling. *Earth and Planetary Science Letters* **90**, 315–329 (1988).

62. Niklas, K. J., Tiffney, B. H. & Knoll, A. H. Patterns in vascular land plant diversification. *Nature* **303**, 614–616 (1983).

63. Dahl, T. W. & Arens, S. K. M. The impacts of land plant evolution on Earth's climate and oxygenation state – An interdisciplinary review. *Chemical Geology* **547**, 119665 (2020).

64. Spencer, C. J., Kirkland, C. L. & Taylor, R. J. M. Strategies towards statistically robust interpretations of in situ U-Pb zircon geochronology. *Geoscience Frontiers* **7**, 581–589 (2016).

65. Spencer, C. J., Kirkland, C. L., Roberts, N. M. W., Evans, N. J. & Liebmann, J. Strategies towards robust interpretations of in situ zircon Lu–Hf isotope analyses. *Geoscience Frontiers* **11**, 843–853 (2020).

66. Liebmann, J., Spencer, C. J., Kirkland, C. L., Xia, X. P. & Bourdet, J. Effect of water on δ18O in zircon. *Chemical Geology* **574**, 120243 (2021).

67. Spencer, C. J. *et al.* Paleoproterozoic increase in zircon δ18O driven by rapid emergence of continental crust. *Geochimica et Cosmochimica Acta* **257**, 16–25 (2019).

68. Jensen, G. *Closed-form estimation of multiple change-point models*. *PeerJ Preprints* (2013) doi:10.7287/peerj.preprints.90v3.

69. Gallagher, K. *et al.* Inference of abrupt changes in noisy geochemical records using transdimensional changepoint models. *Earth and Planetary Science Letters* **311**, 182–194 (2011).

70. Vervoort, J. D. & Kemp, A. I. S. Clarifying the zircon Hf isotope record of crust-mantle evolution. *Chemical Geology* **425**, 65–75 (2016).

71. Roberts, N. M. W. & Spencer, C. J. The zircon archive of continent formation through time. in *Geological Society Special Publication* (eds. Roberts, N. M. W., Van Kranendonk, M. J., Parman, S. W., Shirey, S. B. & Clift, P. D.) vol. 389 197–225 (2015).

72. Budd, G. E. & Mann, R. P. History is written by the victors: the effect of the push of the past on the fossil record. *Evolution* **72**, 2276–2291 (2018).

73. Cunningham, J. A., Liu, A. G., Bengtson, S. & Donoghue, P. C. J. The origin of animals: can molecular clocks and the fossil record be reconciled? *BioEssays* **39**, 1–12 (2017).

74. Dos Reis, M. *et al.* Uncertainty in the timing of origin of animals and the limits of precision in molecular timescales. *Current biology* **25**, 2939–2950 (2015).

75. Husson, J. M. & Peters, S. E. Nature of the sedimentary rock record and its implications for Earth system evolution. *Emerging Topics in Life Sciences* **2**, 125–136 (2018).

76. Donoghue, P. C. J., Harrison, C. J., Paps, J. & Schneider, H. The evolutionary emergence of land plants. *Current Biology* **31**, R1281–R1298 (2021).

77. Roberts, N. M. W. & Spencer, C. J. The zircon archive of continent formation through time. *Geological Society, London, Special Publications* **389**, 197–225 (2015).

78. Spencer, C. *et al.* Disparities in oxygen isotopes of detrital and igneous zircon identify erosional bias in crustal rock record. *Earth and Planetary Science Letters* **577**, 117248 (2022).

Composition of continental crust altered by the emergence of land plants

Christopher J. Spencer[1]*, Neil S. Davies[2], Thomas M. Gernon[3], Xi Wang[1], William J. McMahon[2], Taylor Rae Morrell[1], Thea Hincks[3], Peir K. Pufahl[1], Alexander Brasier[4], Marina Seraine[1], Gui-Mei Lu[1,5]

*Corresponding author. Email: c.spencer@queensu.ca

[1]Department of Geological Sciences and Geological Engineering, Queen's University; Kingston K7L 2N8, Ontario, Canada

[2]Department of Earth Sciences, University of Cambridge; Downing Street, Cambridge CB2 3EQ, United Kingdom

[3]School of Ocean & Earth Science, University of Southampton; Southampton SO14 3ZH, United Kingdom

[4]School of Geosciences, University of Aberdeen, King's College; Aberdeen AB24 3UE, United Kingdom

[5]State Key Laboratory of Geological Processes and Mineral Resources, School of Earth Sciences, China University of Geosciences; Wuhan 430074, China

Extended Data Figures and Tables

This PDF includes:

Extended Data Figures 1-6

Extended Data Table 1

Extended Data Figure Captions

Extended Data Fig. 1: Secular plot of δ^{18}O in mudrocks and zircon during different Periods in the Palaeozoic. Note that no systematic or long-term change in shale composition is present throughout the Phanerozoic. Mudrock δ^{18}O data are from [34,79,80]. Uncertainty bars are 2 S.D.

Extended Data Fig. 2: Transdimensional Markov chain Monte Carlo simulation of the zircon crustal residence versus δ^{18}O slope, r^2, and correlation coefficients demonstrates a statistically valid change point between 450-410 Myr ago with a maximum likelihood at 440 Myr ago (using one million simulations).

Extended Data Fig. 3: Transdimensional Markov chain Monte Carlo (MCMC) simulation and conjugate partitioned recursion (CPR) of the percentage of mudrocks through time. Data from ref. [17]. MCMC yields a statistically valid change point between 430-420 Myr ago with a maximum likelihood at 423 Myr ago (using one million simulations) whereas CPR shows a change point at 430 Myr ago.

Extended Data Fig. 4: Crustal residence time vs $\delta^{18}O$ in zircon through time. This includes (A) the Archean Eon (pre-2500 Myr ago), and major supercontinent assembly events including (B) Nuna from 2200 to 1700 Myr ago, (C) Columbia from 1700 to 1200 Myr ago, (D) Rodinia from 1200-900 Myr ago, Pangea from 400-250 Myr ago, and (F) post-Pangea assembly from 250 Myr ago to present.

Extended Data Fig. 5: Crustal residence versus δ18O in zircon since 720 Myr ago (A-E). It is assumed here that all primary magmas are initially derived from the mantle with a δ18O of ~5.5‰ and a crustal residence time less than ~250 Myr (approximating the depleted mantle compositions 61). The degree of correlation between εHf and $\delta^{18}O_{zircon}$ is markedly different in the latter two panels (A & B), with the panels covering pre-430 Myr ago showing greater degrees of scatter and weak correlations. F) r^2 versus slope of the regression from 700 Myr ago to 0 Myr ago in 10 Myr steps using a rolling window.

Extended Data Fig. 6: Statistical relationship between zircon εHf and $\delta^{18}O$ through time. A step-change algorithm (conjugate partitioned recursion 5) demonstrates a statistically valid step change in the slope, r^2 and correlation coefficients at either 450 Myr ago (linear regression slope and Pearson's Correlation) or 430 Myr ago (r^2 and Spearman's Rank Correlation). The increase in vascular plants at 450 Myr ago and the increase in mudrock percentage at 430 Myr ago are shown as vertical dashed lines.

Extended Data Table 1. (Separate file)

Compiled zircon U-Pb, Lu-Hf, and $\delta^{18}O$ database.

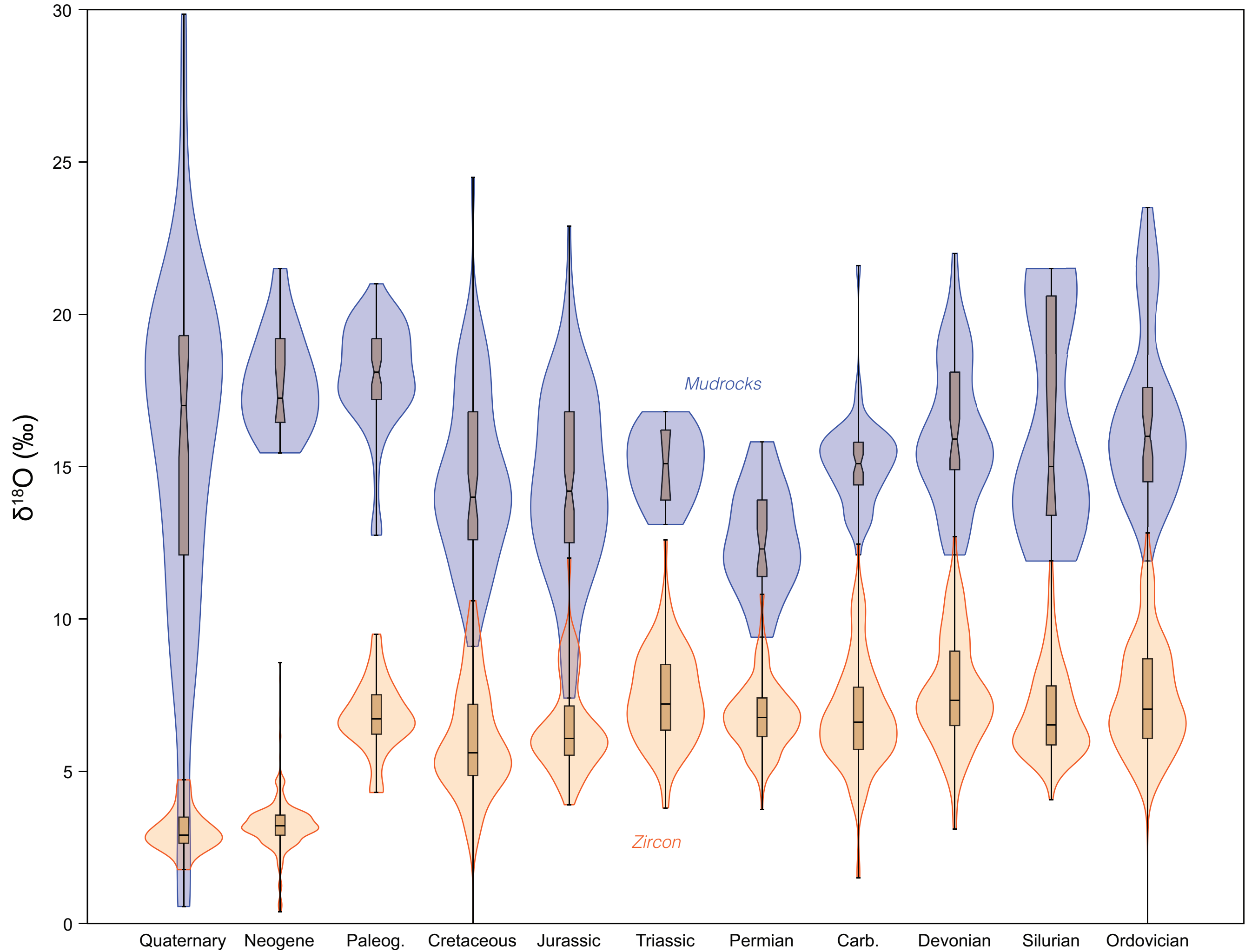

30
25
20
15
10
5
0
δ18O (‰)
Mudrocks
Zircon
Quaternary
Neogene
Paleog.
Cretaceous
Jurassic
Triassic
Permian
Carb.
Devonian
Silurian
Ordovician

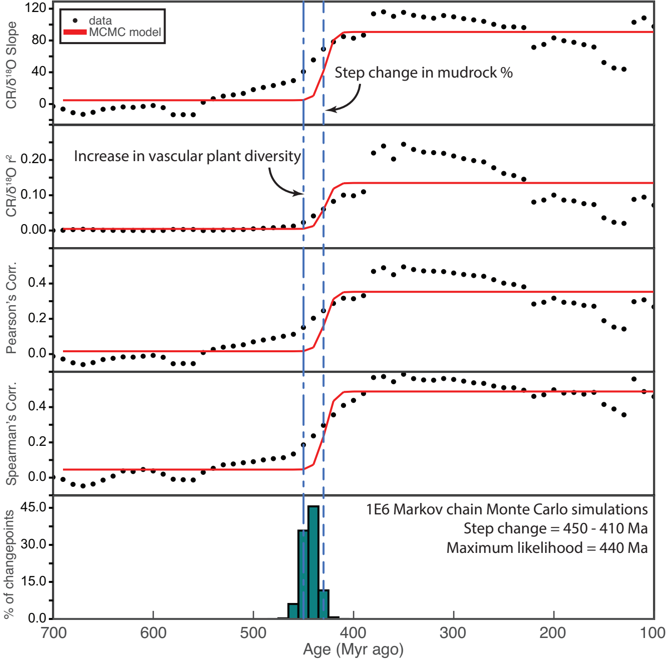
data
MCMC model
Step change in mudrock %
Increase in vascular plant diversity
1E6 Markov chain Monte Carlo simulations
Step change = 450 - 410 Ma
Maximum likelihood = 440 Ma
CR/δ18O Slope
CR/δ18O r2
Pearson's Corr.
Spearman's Corr.
% of changepoints
Age (Myr ago)
120
80
40
0
0.20
0.10
0.00
0.4
0.2
0.0
45.0
30.0
15.0
0.0
700
600
500
400
300
200
100

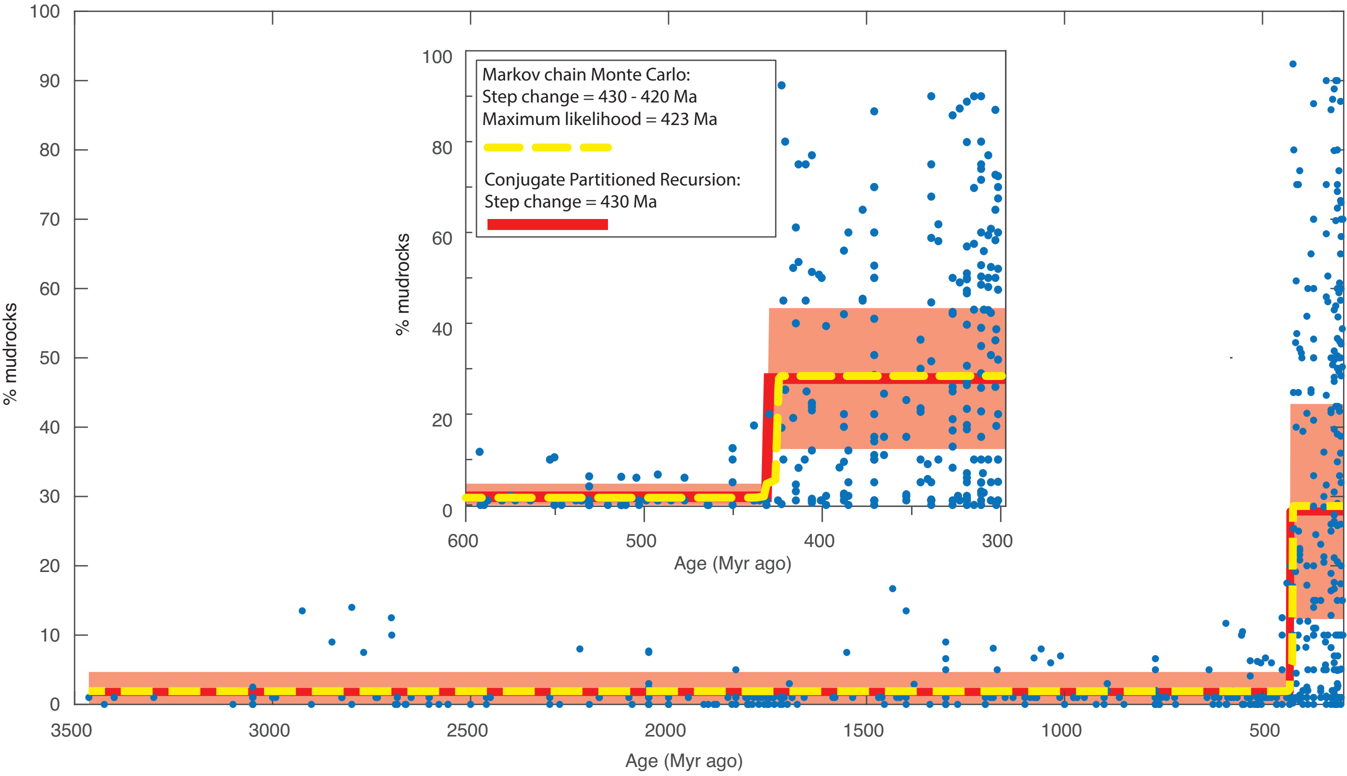

Markov chain Monte Carlo:
Step change = 430 - 420 Ma
Maximum likelihood = 423 Ma
Conjugate Partitioned Recursion:
Step change = 430 Ma
% mudrocks
Age (Myr ago)
100
90
80
70
60
50
40
30
20
10
0
3500
3000
2500
2000
1500
1000
500
600
400
300

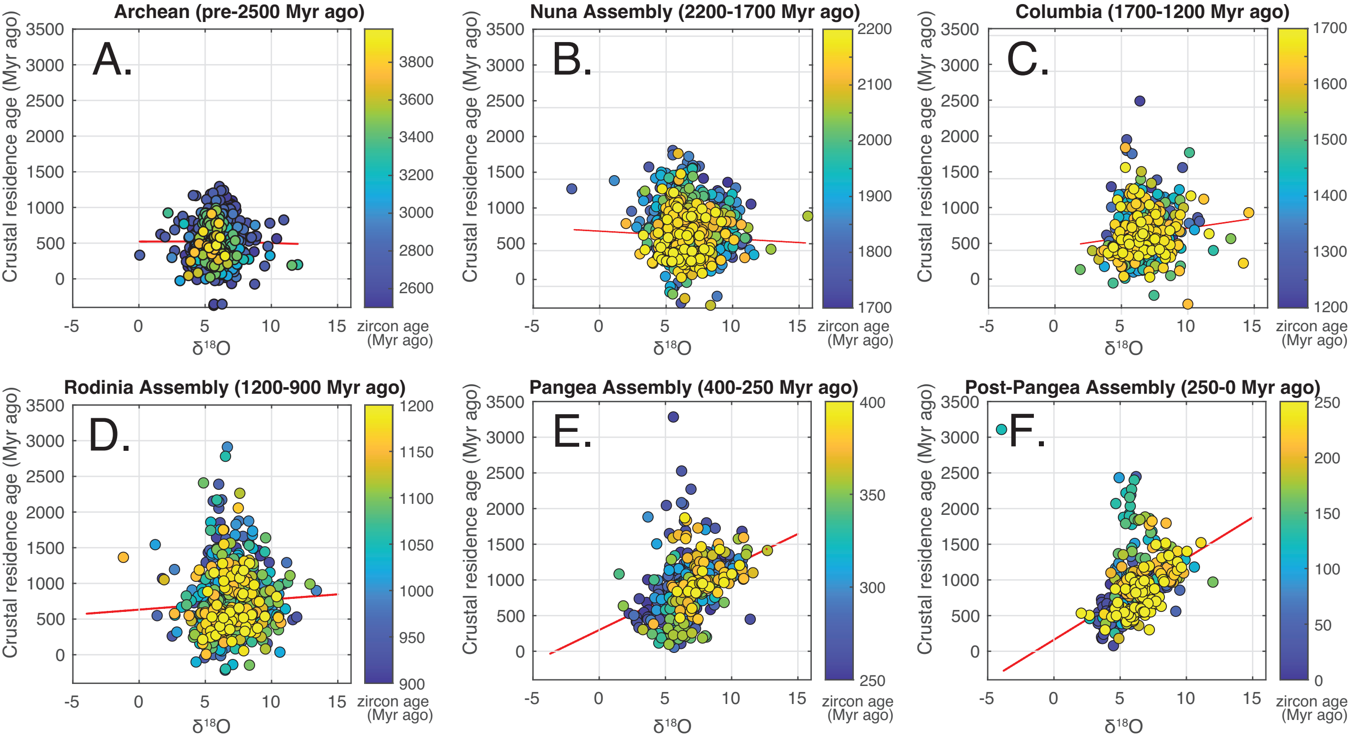
Archean (pre-2500 Myr ago)
A.
Nuna Assembly (2200-1700 Myr ago)
B.
Columbia (1700-1200 Myr ago)
C.
Rodinia Assembly (1200-900 Myr ago)
D.
Pangea Assembly (400-250 Myr ago)
E.
Post-Pangea Assembly (250-0 Myr ago)
F.
Crustal residence age (Myr ago)
δ18O
zircon age (Myr ago)

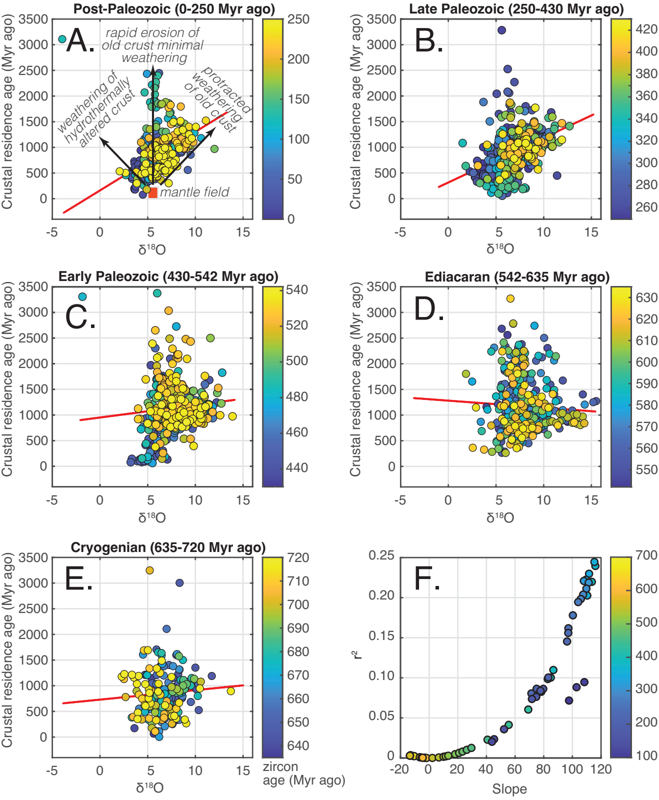

Post-Paleozoic (0-250 Myr ago)
A.
rapid erosion of old crust minimal weathering
weathering of hydrothermally altered crust
protracted weathering of old crust
mantle field
Late Paleozoic (250-430 Myr ago)
B.
Early Paleozoic (430-542 Myr ago)
C.
Ediacaran (542-635 Myr ago)
D.
Cryogenian (635-720 Myr ago)
E.
F.
Crustal residence age (Myr ago)
δ18O
zircon age (Myr ago)
r2
Slope

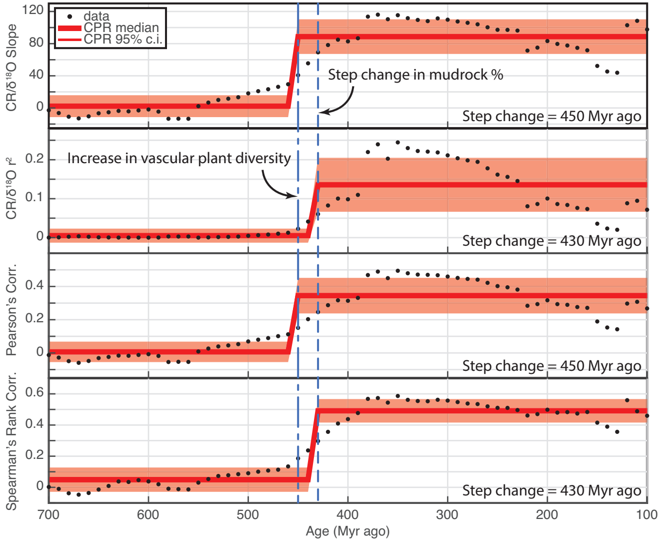
data
CPR median
CPR 95% c.i.
120
80
40
0
CR/δ18O Slope
Step change in mudrock %
Step change = 450 Myr ago
0.2
0.1
0
CR/δ18O r²
Increase in vascular plant diversity
Step change = 430 Myr ago
0.4
0.2
0
Pearson's Corr.
Step change = 450 Myr ago
0.6
0.4
0.2
0
Spearman's Rank Corr.
Step change = 430 Myr ago
700
600
500
400
300
200
100
Age (Myr ago)